RSC Advances

ROYAL SOCIETY
OF **CHEMISTRY**

www.rsc.org/advances

Journal Name

RSC Advances

ARTICLE TYPE

A facile and low cost strategy to synthesize Cd$_{1-x}$Zn$_x$Se thin films for photoelectrochemical performance: Effect of zinc content

Chaitali S. Bagade,[a] Sawanta S. Mali,[b] Vishvanath B. Ghanwat,[a] Kishorkumar V. Khot,[a] Pallavi B. Patil,[a] Suvarta D. Kharade,[a] Rahul M. Mane,[a] Neha D. Desai,[a] Chang K. Hong,[b] Pramod S. Patil[c] and Popatrao N. 5 Bhosale*[a]

In present work we report, a facile chemical route for the deposition of Cd$_{1-x}$Zn$_x$Se thin films by using a simple, self organized arrested precipitation technique (APT). Effect of Zn content on optical, structural, 10 morphological, compositional and photoelectrochemical properties in Cd$_{1-x}$Zn$_x$Se thin films were investigated. The optical properties and band gap profile of Cd$_{1-x}$Zn$_x$Se thin films were varied with respect to Zn content. Estimated direct optical band gap was found to be in the range of 1.77 to 1.98 eV. X-ray diffraction (XRD) studies reveal that films were nanocrystalline in nature with a pure cubic crystal structure and calculated crystallite size lies in the range 36.5 to 66.3 nm. Scanning electron microscopy 15 (SEM) demonstrates that surface morphology can be improved with incorporation of Zn into CdSe lattice. Compositional analysis of all samples was carried out by using energy dispersive X-ray spectroscopy (EDS) and X-ray photoelectron spectroscopy (XPS), it confirms stoichiometric deposition of Cd$_{1-x}$Zn$_x$Se thin films. *J-V* characteristics of all samples were studied in sulphide/polysulphide redox electrolyte. High efficiency 0.68% was observed due to lower crystallite size and higher surface area. These results show 20 that by varying Zn content in Cd$_{1-x}$Zn$_x$Se thin films photoelectrochemical performance can be enhanced.

Introduction

Increasing worldwide demand of energy and limited fossil fuel reserves on the planet earth requires development of reliable, sustainable and renewable energy sources.[1] Various technologies 25 are available, to achieve desired goals from the view point of solar energy conversion and photovoltaic materials are believed to be the cleanest way.[2] The II^B–VI^A semiconductors have been a focal point in this regard, since they offer a spectrum of materials, whose band gap energy cover the entire visible region of solar 30 light spectrum.[3] Due to their superior photoelectrochemical conversion efficiencies it is widely used in the fabrication of solar cells and optoelectronic devices.[4] For economic and large area deposition of solar cell, photoelectrodes of II^B–VI^A semiconductor compounds such as cadmium chalcogenides are 35 highly important. Optical band gap coupled with high absorption coefficients of II^B–VI^A semiconductor results direct consequence of the utilization of various electronic and optoelectronic devices.[5-6] Since binary nanocrystalline semiconductors have fixed band levels such as 1.33 eV (CdTe),[7] 2.2 eV (InSe),[8] 2.4 eV 40 (CdS),[9] 1.48eV (Bi$_2$Se$_3$),[10] it is difficult to find the best semiconductors to form suitable band alignment at the interface with wide band gap semiconductors. This problem can be circumvented by using ternary or quaternary semiconductors such as MoBi$_2$S$_5$,[11] Mo(S,Se)$_2$,[12] Bi$_2$(S,Se)$_3$[13] and MoBi$_2$(Se,Te)$_5$,[14] 45 MoBiInSe$_5$,[15] Cu$_3$SbSe$_4$[16] that possess variable band gap with

change in its chemical composition.

Optical properties, crystal structures and band structures of CdSe and ZnSe are very similar.[17] Therefore the system Cd$_{1-x}$Zn$_x$Se would not only result in the feasibility of a graded energy 50 gap of a broad spectral sensitivity but many more material characteristics.[18] These characteristics can be altered and excellently controlled by the bath composition.[19] CdSe and ZnSe are known to exist in either cubic zinc blende or hexagonal wurtzite crystal forms depending on the composition and the 55 preparative conditions.[20-21] CdSe is n-type semiconductor material with direct band gap energy of 1.74 eV and it is very promising candidate for photoelectrochemical and photo-conductive cells.[22] The ZnSe is very important material for luminescent and light emitting devices.[23-24] However CdSe is 60 found to undergo photocorrosion when used in photoelectrochemical cells, but ZnSe is more stable though less photoactive due to its wide band gap (2.7 eV).[25] Therefore to overcome this shortcomings, coupling of CdSe and ZnSe would provide materials with different band gaps. 65 Depending upon various parameters which will be suitable for accomplishing the twin tasks of increased absorption of solar spectrum and enhanced resistance towards photocorrosion, combination of Cd$_{1-x}$Zn$_x$Se semiconductor material will be beneficial for solar cells.[26-27] 70 Cd$_{1-x}$Zn$_x$Se is a promising ternary material because of its

tunable parameters such as band gap and surface morphology. The most important applications of $Cd_{1-x}Zn_xSe$ thin film is in solar cells,[28] high efficiency thin film transistors,[29] light emitting diodes, laser diodes[30] and electroluminescent devices.[31] $Cd_{1-x}Zn_xSe$ thin films can be prepared by various methods, such as chemical bath deposition (CBD),[32] vacuum evaporation,[33] molecular beam epitaxy (MBE),[34] electrodeposition (ED),[35] metal-organic chemical vapour deposition (MOCVD),[36] etc. Compared to above mentioned deposition techniques, APT is low cost method, in which stoichiometry of deposits can be controlled. Extensive research has been conducted to improve photoelectrochemical performances of $Cd_{1-x}Zn_xSe$ thin films by using water soluble conjugated polymer and annealed films at higher temperature. [37]

Our intention is to employ this material for the fabrication of photovoltaic devices. Therefore as a part of our continuing program we concentrated on our bifocal interest: (i) to develop a suitable method and optimize the different deposition parameters so as to obtain good quality $Cd_{1-x}Zn_xSe$ thin films and (ii) to investigate and analyses the structural, optical and photoelectrochemical properties of synthesized films. In the present investigation, for the first time to report deposition of $Cd_{1-x}Zn_xSe$ thin films on ITO glass substrates by APT to study their optostructural, morphological and photoelectrochemical application.

Experimental

Materials and method

All chemicals used are AR grade and solutions prepared without further purification. Cadmium acetate dihydrate $(Cd(CH_3COO)_2 \cdot 2H_2O)$ (98 %, S D Fine Chem) and zinc acetate dihydrate $(Zn(CH_3COO)_2 \cdot 2H_2O)$ (98 %, S D Fine Chem.), were used as source of Cd and Zn ions. Ethylenediaminetetraacetic acid disodium salt (EDTA) (98 %, S D Fine Chem.) was used as complexing agent. Sodium selenosulphite (Na_2SeSO_3) were used as source of Se which is prepared from selenium metal powder (99 % Sigma Aldrich) and sodium sulphite (Na_2SO_3) (96 %, S D Fine Chem.) by dissolving selenium metal powder in saturated solution of Na_2SO_3 and refluxing whole solution for 8 h.[15] Ammonia (NH_3) (28–30 %, Thomas Baker) was used to maintain pH of the bath. For measuring photoelectrochemical cell properties, we have used sulphide/polysulphide redox electrolyte prepared from sodium sulphide (Na_2S) (55-58 %, Thomas Baker), sodium hydroxide (NaOH) (99 %, S D Fine Chem.) and sulphur powder (99 %, S D Fine Chem.). Indium tin oxide (ITO) coated glass substrates were ultrasonically cleaned using detergent followed by methanol treatment and finally dried in acetone vapours.

Deposition of $Cd_{1-x}Zn_xSe$ thin films

In typical synthesis, appropriate volume of 0.05 M [Cd-EDTA] and 0.2 M [Zn-EDTA] solution was taken in reaction container. pH of mixture was adjusted to 10.4 by drop wise addition of ammonia. Adequate volume of 0.25 M Na_2SeSO_3 solution was added to reaction mixture with constant stirring. Total volume of reaction bath was made to 50 ml by adding double-distilled water then reaction mixture was stirred for 5 min to get homogeneous

solution. Precleaned ITO glass substrates were immersed vertically close to the inner wall of reaction container and then kept for 4 h at 50° C temperature with constant rotation 45 rpm. Formation of good quality thin films depends upon various preparative parameters such as precursor concentration, complexing agent, pH, bath temperature and deposition time. After optimised deposition parameters substrates were withdrawn from bath, sufficiently rinsed with double distilled water and dried at room temperature. Deposited films were uniform, peach color and adherent to glass substrate. Further in order to check effect of Zn content, different volume of Zn were added in reaction bath as shown in Table 1. Deposited films were correspondingly designated x = 0.0, 0.2, 0.4, 0.6 and 0.8 respectively, for different zinc composition. These films were used for further investigations.

Table 1 Preparative parameters for the synthesis of the $Cd_{1-x}Zn_xSe$ thin films, pH = 10.4, temperature = 50 ^{0}C.

Sr. No	Sample code	Samples	Bath composition		
			Volume of 0.05 M Cd (ml)	Volume of 0.2 M Zn x (ml)	Volume of 0.25 M Se (ml)
1	x = 0.0	CdSe	20	00	20
2	x = 0.2	$Cd_{0.8}Zn_{0.2}Se$	16	04	20
3	x = 0.4	$Cd_{0.6}Zn_{0.4}Se$	12	08	20
4	x = 0.6	$Cd_{0.4}Zn_{0.6}Se$	08	12	20
5	x = 0.8	$Cd_{0.2}Zn_{0.8}Se$	04	16	20

Characterizations of thin films

Thickness of the deposited thin films was measured by surface profiler (AMBIOS XP-1). UV–Vis Spectrophotometer (Model: Shimadzu UV-1800) was used to record absorption spectra of deposited thin films in the wavelength range 400–1100 nm. Structural properties of thin films were studied using X-ray Diffractometer (Bruker AXS, D8 Model) using Cu Kα (λ =1.5418 Å) radiation for 2θ ranging from 10º to 80º. Surface morphology and elemental analysis were examined using Scanning Electron Microscope (SEM) equipped with Energy Dispersive Spectroscopic (EDS) analyzer (JEOL-JSM-6360A). Valance state information concerning thin film was studied using X-ray Photoelectron Spectroscopy (XPS, Thermo Scientific, Multilab-2000) with a multi-channel detector, which can endure high photon energies from 0.1–3.0 keV. Photoelectrochemical (PEC) measurement was carried out by using $Cd_{1-x}Zn_xSe$ thin film as photoanode in dark and under illumination using a 500 W tungsten filament lamp (intensity 30 mWcm^{-2}) at electrochemical workstation (AUTOLAB PGSTAT 100 potentiostat). Photoelectrochemical cell was a two electrode system: $Cd_{1-x}Zn_xSe$ film deposited on ITO substrate is a working electrode with active surface area of 1cm^2 and graphite as counter electrode in sulphide/polysulphide as redox electrolyte.

Results and Discussion

Growth mechanism of thin film formation-

Bath containing metal EDTA ion complexes allows to control release of Cd^{2+} and Zn^{2+} ions in reaction bath. Decomposition of sodium selenosulphite in an aqueous alkaline medium releases Se^{2-} ions. Deposition process is based on slow release of Cd^{2+},

Journal Name

ARTICLE TYPE

Zn^{2+} and Se^{2-} ions in the solution and ion by ion condensation of released ions onto the substrate surface. Concentration of Cd-EDTA and Zn-EDTA complexed ions in a reaction bath controls rate of nucleation and consequently rate of deposition. Upon
5 release of Cd^{2+} and Se^{2-} ions, supersaturation of CdSe is readily obtained because of its low solubility product. Formation of ZnSe proceeds similarly but deposition of $Cd_{1-x}Zn_xSe$ is complicated due to difference in reactivity of Cd^{2+} and Zn^{2+} and solubility products of CdSe and ZnSe. The solubility product of CdSe $\cong 10^{-}$
10 ^{33} is smaller than ZnSe $\cong 10^{-31}$ which leads to faster nucleation and growth of CdSe as compared to ZnSe.[33] Therefore successful deposition of $Cd_{1-x}Zn_xSe$ films requires a much higher concentration of free Zn^{2+} ions than free Cd^{2+} ions to reach supersaturation for both phases.[38] We achieved this condition by
15 using much higher concentration of Zn salt, although complexing agent with higher affinity for Cd than Zn could also be effective.

Scheme 1 Possible growth mechanism for deposition of $Cd_{1-x}Zn_xSe$ thin. films

20 Basically in APT complexing agents arrest the metal ion and release them slowly which is to be deposited on the substrate surface. In APT rate of reaction between metal ions with chalcogen can be controlled by using suitable complexing agent in this case we have used EDTA. An increase in the deposition
25 temperature favours homogenous precipitation rather than film formation which causes saturation. Best condition in the deposition process for yielding good quality thin films is at 50^oC for 4h. Formation of $Cd_{1-x}Zn_xSe$ thin films by varying zinc content proceeds via following steps,
30 Formation of EDTA complex of Cd^{2+} and Zn^{2+} takes place in aqueous medium where EDTA used is disodium salt is as shown in eq. (1) and (2)

$$Cd\,(CH_3COO)_2 + EDTA \longrightarrow [Cd\,(EDTA)]^{2+} + 2CH_3COONa \quad (1)$$

$$Zn\,(CH_3COO)_2 + EDTA \longrightarrow [Zn\,(EDTA)]^{2+} + 2CH_3COONa \quad (2)$$
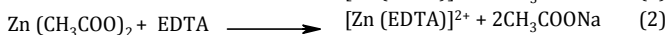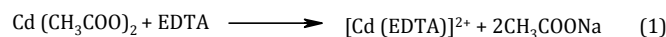
Slowly release of Cd^{2+} and Zn^{2+} ions takes place at optimum pH
35 and temperature shown in eq. (3) and (4)

$$[Cd\,(EDTA)]^{2+} \longrightarrow Cd^{2+} + EDTA \quad (3)$$

$$[Zn\,(EDTA)]^{2+} \longrightarrow Zn^{2+} + EDTA \quad (4)$$
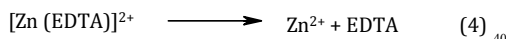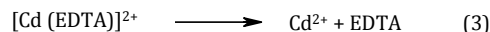
40 According to eq. (5) and (6) Se^{2-} ions release in the alkaline medium due to the hydrolysis of sodiumselenosulphite as follows

$$Na_2SeSO_3 + OH^- \xrightarrow{pH\ 10.4} Na_2SO_4 + HSe^- \quad (5)$$

$$HSe^- + OH^- \longrightarrow Se^{2-} + H_2O \quad (6)$$
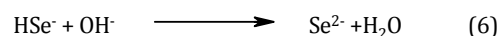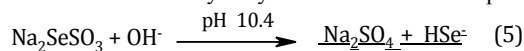
Overall reaction was in eq. (7)

$$Cd^{2+} + Zn^{2+} + Se^{2-} \xrightarrow[pH\ 10.4]{50^0C} Cd_{1-x}Zn_xSe \quad (7)$$
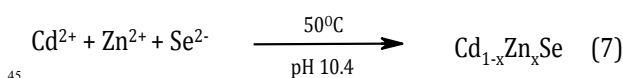
45 When ionic product, exceeds the solubility product precipitation occurs. The deposition of material takes place by ion by ion condensation process followed by Ostwald ripening process on substrate surface. In ion-by-ion condensation of thin films,
50 adsorption of metal ions on the surface substrate is an important step which forms the nucleation centres. As a result, there are large number of small nuclei centres are formed upon which growth process can take place.[39] The smaller crystals act as nutrient for the bigger crystals. As the larger crystals grow, area
55 around them is depleted by smaller crystals. Larger particles grow at the expenses of smaller particles on the basis of the Ostwald ripening law. [12,40] The schematic of formation of $Cd_{1-x}Zn_xSe$ thin films is shown in scheme 1. Deposited thin films were uniform and well adhered to the substrate surface.

60 **Thickness measurement**

Thicknesses of deposited thin films were found to be 540 to 730 nm with varying bath composition. Thickness of the deposited films is controlled by two independent variables such as uniform growth and surface morphology. The process of precipitation of a
65 substance in the solution depends on degree of supersaturation[41] and formation of nucleus and its growth onto substrate surface. From Fig 1 it is clearly seen that film thickness of $Cd_{1-x}Zn_xSe$ thin film increases with increasing zinc content. Especially in our case precipitation and growth of films depends on the degree of
70 supersaturation of both CdSe and ZnSe. The ZnSe having higher degree of supersaturation than CdSe. Concentration of Zn^{2+} ions is much high in the bath as compared to Cd^{2+} thus with increasing Zn content maximum growth rate of films takes place. Which may leads to increases in film thickness.[42-43] Also this may be
75 attributed due to the strong ionic bonding between zinc and selenium as compared to weak ionic bonding between cadmium and selenium. Strong ionic bonding between Zn^{2+} and Se^{2-} increase the film thickness as number of Zn^{2+} ions increases.[10,]
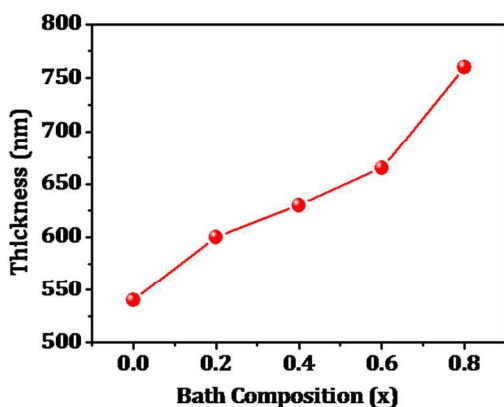
Fig.1 Plot of film thickness as function of $Cd_{1-x}Zn_xSe$ bath composition.

Optical absorption study

Optical band gap energy of $Cd_{1-x}Zn_xSe$ films were calculated by using optical absorption spectra. Optical absorption spectra of deposited $Cd_{1-x}Zn_xSe$ thin films were recorded in wavelength range 400-1100 nm, as shown in Fig. 2a. Electronic transition between valence and conduction bands starts at the absorption edge corresponding to the minimum energy difference between the lowest energy of conduction band and highest energy of valence band in material. The positions of fundamental absorption edge get shifted to higher wavelength with increasing Zn content. Fig 2a clearly shows that maximum optical absorption is observed at around 600-700 nm.

To determine the energy band gap values, we plotted $(\alpha h\nu)^2$ versus $(h\nu)$ which is based on eq. (8)

$$\alpha = \frac{A(h\nu - Eg)^n}{h\nu} \qquad (8)$$

where 'α' is absorption coefficient, '$h\nu$' is photon energy 'A' is a parameter that depends on the transition probability, 'h' is planck's constant, 'Eg' is optical band gap energy of the material and exponent 'n' depends on nature of transition during absorption process. The value of n is ½, 3/2, 2, 3 for direct allowed, direct forbidden, indirect allowed and indirect forbidden transitions, respectively. The band gap of $Cd_{1-x}Zn_xSe$ thin films was determined by extrapolating straight line to the energy axis. Nature of plots suggest a direct and allowed type of transition[44] since line dependence is obtained at n = ½ . Fig.2b shows optical band gap values of $Cd_{1-x}Zn_xSe$ thin film varied from 1.77 to 1.98 eV with respect to zinc content. The energy band gaps of $Cd_{1-x}Zn_xSe$ films are owing to similar band structures of two compounds with x value increases between two limits.[45] The enhancement in band gap is not only because ZnSe has higher band gap than CdSe but also may be due to zinc content attributed to a real band gap change between CdSe and ZnSe. [46] Which also causes an increase in band gap. [47-48] As it is well known, band gap of the ternary compound semiconductors i.e. $Cd_{1-x}Zn_xSe$ linearly dependent on the individual band gap of the materials forming the ternary semiconductor compound.[49] In the present case, it depends on the CdSe and ZnSe band gaps.[50] High absorption coefficient and tunable band gap of $Cd_{1-x}Zn_xSe$ thin films will add advantages in respect of their application in

photovoltaic devices.[48]
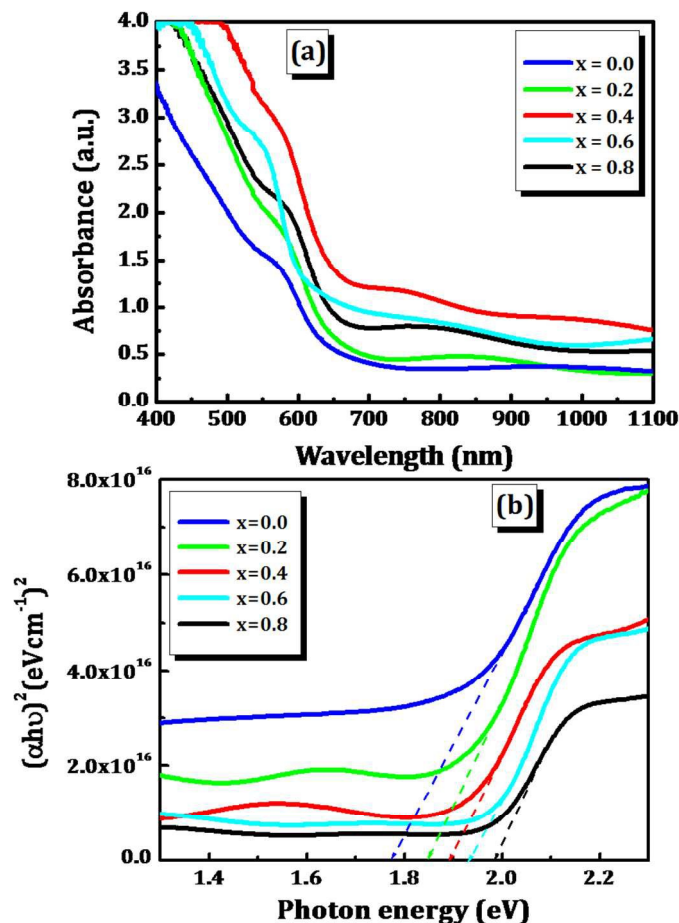
Fig. 2 (a) Optical absorption spectra and **(b)** Plots of $(\alpha h\nu)^2$ *vs.* Photon energy $(h\nu)$ of $Cd_{1-x}Zn_xSe$ (x = 0.0, 0.2, 0.4, 0.6 and 0.8) thin films.

Structural analysis

XRD is an efficient tool for structural analysis of crystalline materials. XRD patterns of $Cd_{1-x}Zn_xSe$ thin films as a function of different zinc content (x) was carried out at room temperature in the range of 10-80° and shown Fig.3a. Broad and intense peaks in XRD patterns confirm nanocrystalline nature of sample. XRD patterns of thin films exhibit peaks at 25.39°, 42.17°, 49.74° and 60.85° which are indexed to the (111), (220), (311) and (400) planes respectively of cubic CdSe (JCPDS card no. 19-0191). Also the peaks at 12.47°, 14.30° and 20.55° are indexed to the (111), (200) and (220) planes of cubic ZnSe (JCPDS card no. 02-0479). The XRD patterns of $Cd_{1-x}Zn_xSe$ nanocrystals were located between those for CdSe and ZnSe materials. Such phase formation of CdSe and ZnSe provides strong evidence of $Cd_{1-x}Zn_xSe$ solid solution formation which was in good agreement with the reported value.[51-55] The kinetics of the alloying mechanism involves dissociation of Zn–Se bonds and diffusion of Zn into CdSe. Zn has important role depending upon concentration when incorporated into the lattice of CdSe, it has strong tendency of replacing Cd from the lattice because of Zn having small ionic radius (1.18 Å) releative to that of Cd (1.36

Journal Name

Dynamic Article Links ▶

ARTICLE TYPE

Å).[56-57] For Zn dominant films, CdSe slightly shifts the peak (111) position towards lower 2θ values confirm the solid solution formation in this region as shown in Fig. 3b and c. Similarly other peaks of cubic ZnSe (111) are also found to be less shift towards

5 higher 2θ values.[58-59] The dependence of the diffraction peak positions of the obtained ternary nanocrystals on their corresponding compositions, which provides an alloying evidences.[50,60-61]
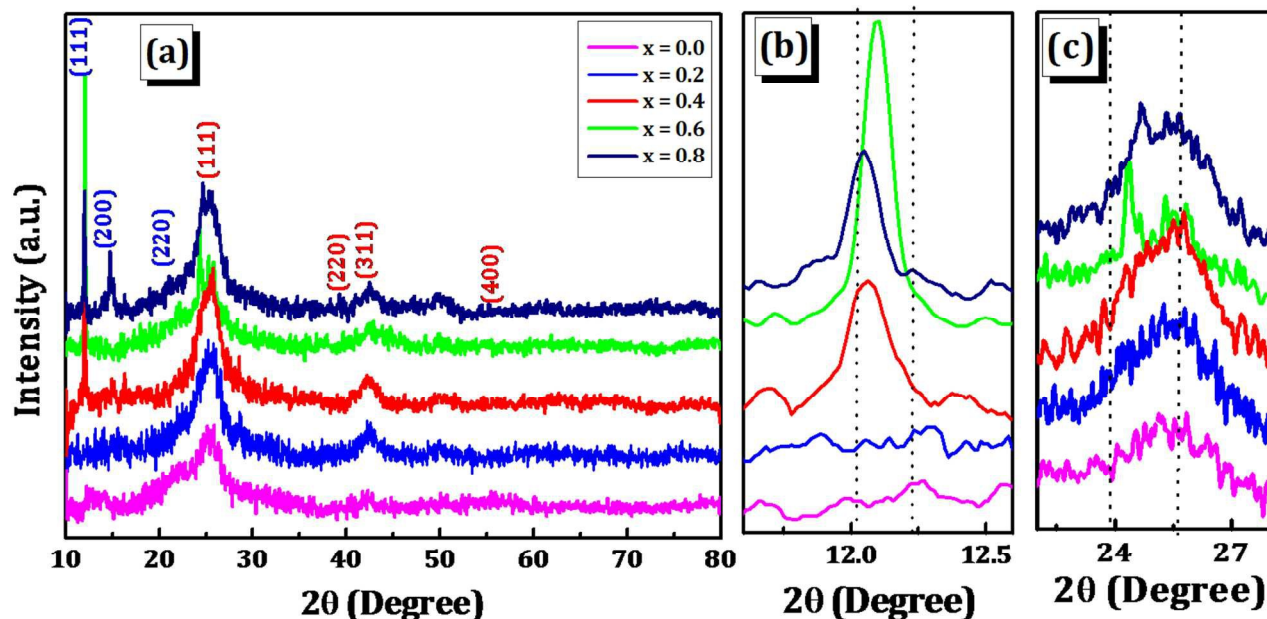
Fig.3 (a) XRD patterns of $Cd_{1-x}Zn_xSe$ thin films (b,c) shifting pattern of $Cd_{1-x}Zn_xSe$ thin films.

10

The average crystallite size (D) was calculated from XRD patterns using Debye scherrer's eq. (9)

$$D = \frac{0.94\lambda}{\beta\cos\theta} \quad 15 \qquad (9)$$

where 'λ' is used X-ray wavelength (1.5406 Å), 'β' is full width of half-maximum (FWHM) in radians and 'θ' is Bragg's angle. The average crystallite size of $Cd_{1-x}Zn_xSe$ (x = 0.0, 0.2, 0.4, 0.6 20 and 0.8) was varied from 36.5 to 66.4 nm. It was observed that crystallite size decreases after increasing Zn content, which indicates that Zn can restrain agglomeration of CdSe nanocrystal and improve surface area of $Cd_{1-x}Zn_xSe$ particles.[11] Such nanocrystalline nature suppresses electron hole pair 25 recombination which is beneficial for enhancement in the PEC performance.[62]

The lattice parameters for the cubic crystal structure were calculated using the following eq. (10)

$$\frac{1}{d^2} = \left(\frac{h^2 + k^2 + l^2}{a^2}\right) \quad 30 \qquad (10)$$

The average lattice parameters for cubic structure (a=b=c) were found to be 4.260 Å and 5.610 Å for $Cd_{1-x}Zn_xSe$ thin films. These lattice parameters are in good agreement with the standard 35 JCPDS data. From calculated values of crystallite size,

dislocation density (δ) and microstrain (ε) for all samples (x = 0.0, 0.2, 0.4, 0.6 and 0.8) were determined by using eq. (11) and (12) respectively and results are listed in Table 2.

$$\delta = \left(\frac{1}{D^2}\right) \qquad (11)$$

40

$$\varepsilon = \left(\frac{\beta\cos\theta}{4}\right) \qquad (12)$$

45 As seen in Table 2 crystallite size decreases whereas dislocation density and microstrain increases. This enhancement is due to the atomic radius of Zn is less than atomic radius of Cd, which strongly affects on structural parameters with increased Zn content. [33]

50 Table **2** Values for crystallite size (D), dislocation density (δ) and microstrain (ε) of the $Cd_{1-x}Zn_xSe$ thin films

Sample	Crystallite size (D) nm	Dislocation density (δ) 10^{-4}(lines m^{-2})	Microstrain (ε) (lines m^{-4})
x = 0.0	66.4	2.2	5.30
x = 0.2	63.0	2.5	5.50
x = 0.4	56.0	3.1	6.18
x = 0.6	43.3	5.3	7.99
x = 0.8	36.5	7.5	9.49
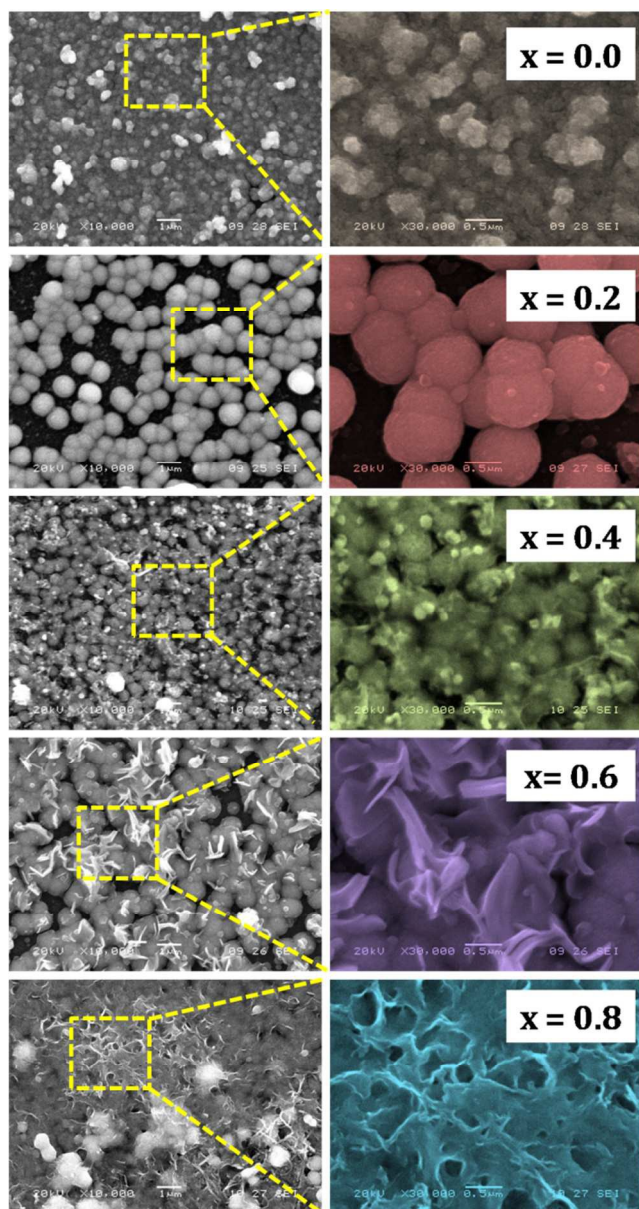
Fig.4 Low and high magnification SEM images of $Cd_{1-x}Zn_xSe$ (x = 0.0, 0.2, 0.4, 0.6 and 0.8) films.

5 **Morphological analysis**

In order to study the microstructures of $Cd_{1-x}Zn_xSe$ thin films, scanning electron microscopy analysis was performed. It is well known that surface properties of thin films influences their optostructural and electrical properties and which is important
10 aspect in application of optoelectronic and solar cell devices. Thus it is very important to investigate surface morphology of the thin films. Fig 4 shows low and high magnification SEM images of $Cd_{1-x}Zn_xSe$ thin films. SEM results show change in surface morphology with respect to zinc content. In Fig 4 x = 0.0 sample
15 show formation of densely packed smooth homogenous surface. Formation of small grains having average size 80 nm and dispersed uniformly on substrate surface. When Zn is merged in CdSe lattice, change in morphology observed with heterogeneous

surface with different shapes and sizes. Sample x = 0.2 clearly
20 reveals formations of nanosphere like structure. As Zn content increases in x = 0.4 nanospheres get diffused to each other to form a spongy nanoball like morphology. It also shows that formation of secondary nanopetal like structure start to grow on surface of nanoballs. These nanopetals clearly differentiated in x
25 = 0.6 sample. Upon increasing Zn content nanosphere with numerous nanopetal like morphology was evaluated in x = 0.6 sample. This morphology may provide high solar conversion efficiency due to large surface area for the absorption of light. With further increase in Zn content a network of interconnected
30 nanofibers was formed over surface as shown for x = 0.8 sample.

Energy dispersive X-ray spectroscopy

Stoichiometry of thin films was determined by using EDS analysis. Fig. 5 shows typical EDS spectra for various zinc
35 contents. The three peaks at 3.55, 1.10 and 1.70 keV confirm the presence of Cd, Zn and Se elements respectively in deposited thin film. From EDS spectra it was observed that intensity of Zn peak increases with increasing zinc content in film. It is difficult to maintain stoichiometriy of elements due to different reactivity of
40 Cd and Zn element and also solubility difference for both phases hence the Cd and Zn atoms could be not uniformly dispersed in atomic level. We achieved nearly stoichiometriy $Cd_{1-x}Zn_xSe$ thin films by varying the volume of Cd and Zn respectively. The actual and observed atomic percentage determined from chemical
45 formula was shown in Table 3.

Table 3 Elemental composition of $Cd_{1-x}Zn_xSe$ (x = 0.0, 0.2, 0.4, 0.6 and 0.8) thin films determined from EDS analysis.

Material	Expected Atomic %			Observed Atomic %		
	Cd	Zn	Se	Cd	Zn	Se
x = 0.0	50.0	0.00	50.0	49.80	0.00	50.22
x = 0.2	40.0	10.0	50.0	40.53	8.71	50.76
x = 0.4	30.0	20.0	50.0	31.46	18.48	50.06
x = 0.6	20.0	30.0	50.0	20.32	29.21	50.47
x = 0.8	10.0	40.0	50.0	11.42	38.55	50.03

50 **Compositional analysis**

The valence state of $Cd_{1-x}Zn_xSe$ thin films was confirmed by XPS analysis. Fig. 6 illustrates survey spectrum and core level spectrum obtained for x = 0.6 sample. As peaks observed in survey spectrum (fig.6a) which confirms presence of cadmium
55 (Cd), zinc (Zn), selenium (Se), carbon (C) and oxygen (O). The position of the C (1s) peak was taken as a standard reference with a binding energy of 284.6 eV.[29] The presence of O (1s) in survey spectrum may be due to atmospheric oxygen. Fig. 6b show high resolution core level spectrum of Cd3d. The two peaks located at
60 binding energy 411.98 eV and 405.02 eV corresponding to the $Cd(3d_{5/2})$ and $Cd(3d_{3/2})$ respectively of Cd^{2+}. Two Zn2p peaks at 1045.08 eV and 1021.03 eV in Fig. 6(c) correspond to Zn $2p_{3/2}$ and Zn $2p_{1/2}$ confirms presence of Zn^{2+}. The corresponding binding energy values of Zn^{2+} can be attributed to Zn–Se bonding
65 in the bulk ZnSe crystal.[63] The core level spectrum for Se (3d) was fitted yielding a single peak at the binding energy of 54.03 eV confirms selenide phase in metal chalcogenides, which is well

RSC Advances

ARTICLE TYPE

agreement with values reported for Se^{2-} phase.[64] The Se 3d singlet peak is significantly broadened over a range of ~6 eV and it include Se $3d_{5/2}$ and $3d_{3/2}$ due to apparent lack of

distinguishable peaks.[65] The values of binding energies for Cd,
5 Zn and Se confirms valance states as Cd^{2+}, Zn^{2+} and Se^{2-} respectively.
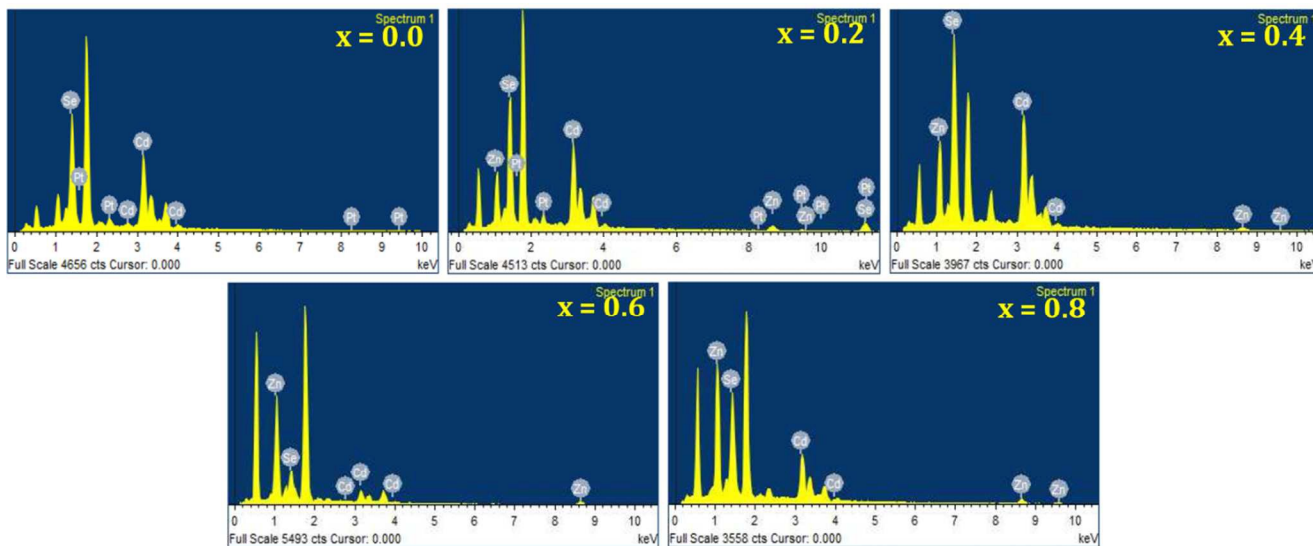
Fig.5 EDS spectra of $Cd_{1-x}Zn_xSe$ (x = 0.0, 0.2, 0.4, 0.6 and 0.8) thin film for various compositions.

10
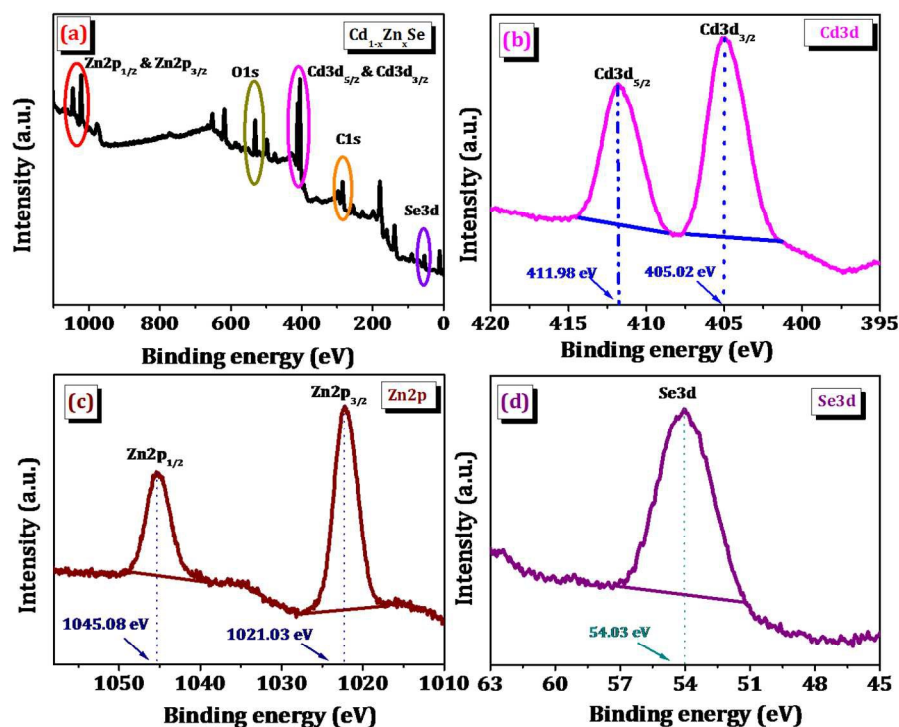
Fig.6 (a) XPS survey spectrum of the $Cd_{1-x}Zn_xSe$ thin film, (b) high-resolution core level XPS spectrum of Cd, (c) high-resolution core level XPS spectrum of Zn, (d) high-resolution core level XPS spectrum of Se.

Photoelectrochemical performance

PEC performance of all $Cd_{1-x}Zn_xSe$ thin films deposited with different composition was checked with the help of standard two
[5] electrode configuration in dark and under illumination of 500 W tungsten filament lamp having light intensity 30 mWcm^{-2} in sulphide/polysulphide redox electrolyte. The current density–voltage *(J–V)* characteristics of glass/ITO/$Cd_{1-x}Zn_xSe$/electrolyte/graphite were measured. For all the samples, *J–V*
[10] characteristic curves in dark display diode like rectifying characteristics. Upon illumination, magnitude of open circuit voltage (*Voc*) increases with negative polarity towards the $Cd_{1-x}Zn_xSe$ electrode, indicating cathodic behaviour of photovoltage which confirms that $Cd_{1-x}Zn_xSe$ thin films are n-type. Output
[15] parameters of PEC solar cell i.e. light conversion efficiency (η%) and fill factor (FF) were calculated from eq. (13) and (14), respectively

$$FF = \left(\frac{J_{max} \times V_{max}}{J_{sc} \times V_{oc}} \right) \quad (13)$$

$$\eta(\%) = \left(\frac{J_{sc} \times V_{oc}}{P_{in}} \times FF \times 100 \right) \quad (14)$$

[20] Where '*Jsc*' is the short-circuit current density and '*Voc*' is the open circuit voltage. '*Jmax*' and '*Vmax*' are the maximum current density and the maximum voltage, and '*Pin*' is the input light intensity (30 m Wcm^{-2}). The detailed PEC cell performance and parameter of $Cd_{1-x}Zn_xSe$ (x = 0.0, 0.2, 0.4, 0.6 and 0.8) thin films
[25] samples are summarized in Table 4. From the *J–V* measurements, the obtained values of *Jsc, Voc, Jmax, Vmax* and FF are shown in Table 4.

Table 4 Solar cell parameters of the $Cd_{1-x}Zn_xSe$ (x = 0.0, 0.2, 0.4, 0.6 and 0.8) thin films

Sample	*Jsc* (mA cm^{-2})	*Voc* (mV)	*Jmax* (mA cm^{-2})	*Vmax* (mV)	*FF*	η(%)
x = 0.0	0.884	577	0.636	267	0.33	0.56
x = 0.2	1.023	584	0.643	273	0.29	0.58
x = 0.4	0.988	585	0.670	282	0.32	0.63
x = 0.6	**1.137**	**580**	**0.666**	**310**	**0.31**	**0.68**
x = 0.8	0.869	583	0.662	274	0.35	0.60

[30] Amongst various compositions, films with composition x = 0.6 was exhibited maximum photo output in polysulphide compared to other photoelectrodes.

When a semiconductor is placed in contact with an electrolyte, electric current initially flows across the junction until electronic
[35] equilibrium is reached, where fermi energy of the electrons in solids (E_F) is equal to redox potential of the electrolyte (E_{redox}). Scheme 2 shows band bending in the dark. This must results an equilibrium distribution of charge among the space-charge region. The diffusion layer is inner Heltmholz plane and inner
[40] surface states. On illumination electron-hole pairs are generated, holes move to the surface of semiconductor and oxidize the electrolyte species while electrons move deep into the bulk of semiconductor and reduce the oxidized species at the counter electrode, thus allowing the redox reactions to occur.[66] When the
[45] illuminated cell is shorted, this situation causes current flow in the external circuit from the counterelectrode to the semiconductor electrodes, thereby making the better carry out an anodic reaction (15)

[50]
$$2S^{2-} \longrightarrow S_2^{2-} + 2e^- \quad (15)$$
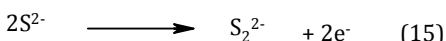
Since holes are regarded as a separate species and have accumulated near interface of anodic reaction (16)

$$2S^{2-} + 2h^+ \longrightarrow S_2^{2-} \quad (16)$$

[55]
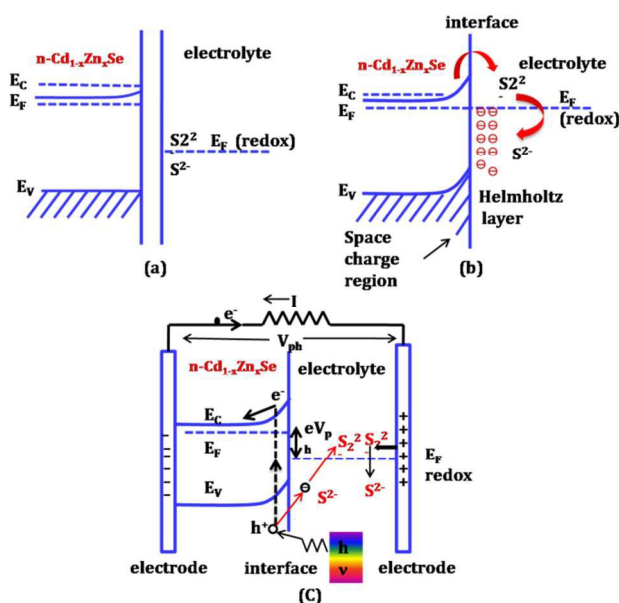
Scheme 2 Explicity and possibility of an electrochemical reaction and generation of electron and holes by means of illumination.

The photocurrent obtained for x = 0.0 sample is relatively
[60] lower, i.e. 0.884 mA cm^{-2} due to recombination of photo generated electrons in n-type CdSe thin films with holes or leak out into the electrolyte, instead of flowing through the external circuit resulting lower efficiency.[47,53] The improvement in conversion efficiency with increasing in Zn content can be
[65] explained on the basis of surface morphology of $Cd_{1-x}Zn_xSe$ thin films. It was observed that x = 0.6 sample shows better performance as compared to x = 0.8 sample. Improvement in performance of x = 0.6 sample seems due to sufficient surface

area to increases the interfacial reaction sites.[67] Closely packed nanopetals improve the carrier transport mechanism and minimize surface trap states. Such types of interconnected nanospheres with petals provide higher effective surface area for light absorption. The numerous pores existed amongst spheres and petals by their interconnection make an intimate contact between material and electrolyte. This type of surface provides a direct path for electron transfer in electrolyte and improves its suitability as photoelectrode in PEC solar cell. This type of double layered structure with scattering layer is beneficial for improved conversion efficiency of solar cell.[62] It is also observed that there is good connection between nanospheres and nanopetals which offers abundant transfer pathway for photogenerated electrons. An interconnected nanofibers like morphology over the surface was observed in case of x = 0.8 sample. Lower efficiency for x = 0.8 was observed by virtue of recombination problems due to the existence of considerable grain boundaries in the film. Therefore electron trapping at the surface and inter grain boundaries result in lower light conversion efficiency.[68] From the above observations, it is clear that PEC performance could be enhanced by improving stability of CdSe coupled ZnSe photo electrodes for better conversion efficiency in solar cell devices.
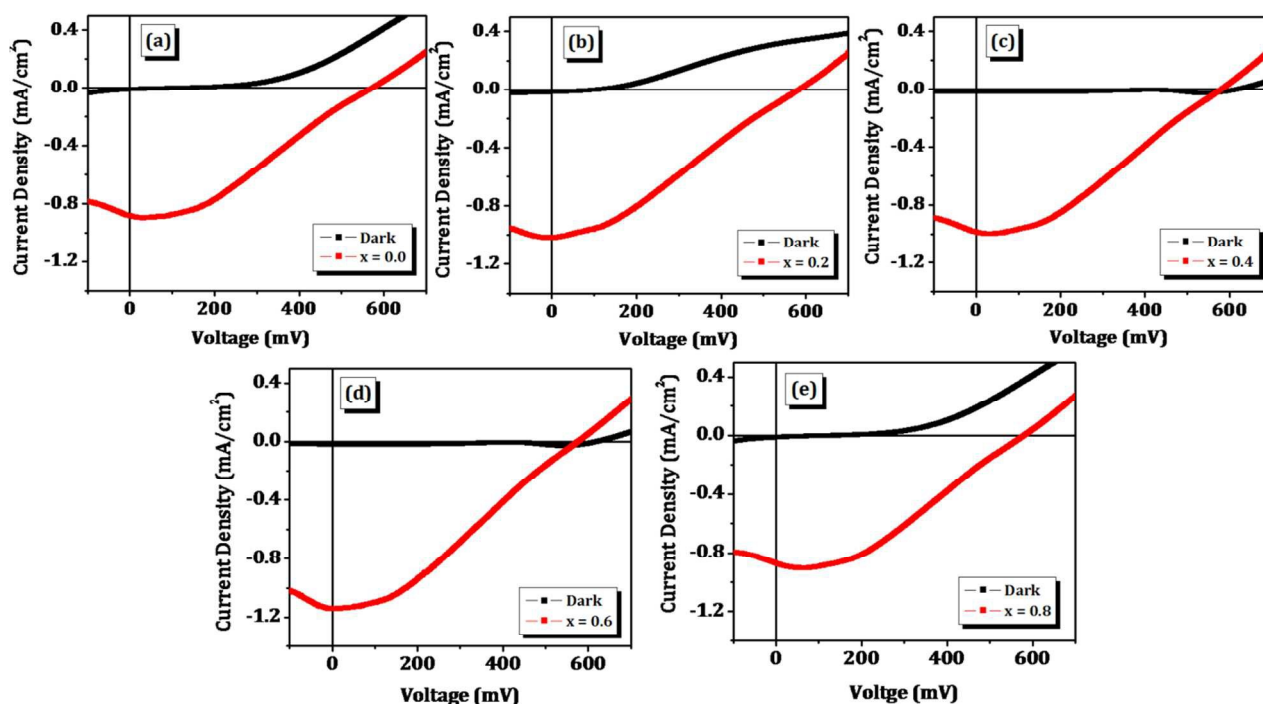
Fig. 7 *J-V* characteristics of $Cd_{1-x}Zn_xSe$ (x = 0.0, 0.2, 0.4, 0.6 and 0.8) thin films in sulphide/polysuphide electrolyte.

Conclusions

In conclusion, we report a facile chemical route for the deposition of $Cd_{1-x}Zn_xSe$ (x = 0.0, 0.2, 0.4, 0.6 and 0.8) thin films by using a simple and cost effective APT. Influence of Zn content on the optostructural, morphological and photoelectrochemical properties of $Cd_{1-x}Zn_xSe$ thin films was investigated. From optical measurements, we can conclude that optical band gap is direct allowed type and varied from 1.77 to 1.98 eV. X-ray diffraction pattern illustrate cubic crystal structure for both CdSe and ZnSe phases and intensity of diffraction peaks increases indicating the incorporation of Zn in CdSe lattice. SEM study illustrated that formation of grain like morphology was observed for CdSe while with increasing Zn content in thin films; morphological transition from nanospheres to interconnected nanopetals was observed. Such morphology shows high efficiency due to large surface area for the absorption of light. EDS and XPS analysis shows presence of all elements (Cd, Zn and Se) in stoichiometric form. The conversion efficiency of the fabricated solar cell was found to increases from 0.56 to 0.68 %. The highest conversion efficiency was obtained for $Cd_{0.4}Zn_{0.6}Se$ (0.68 %) thin film. It was found that the change in composition has significant effect on solar efficiency. Overall achieved results reveals that newly devised APT is a suitable method for the synthesis of different metal chalcogenide thin films.

Notes and references

a Materials Research *Laboratory, Department of Chemistry, Shivaji University,Kolhapur, India. E-mail: p_n_bhosale@rediffmail.com; Fax:+91-231-2691533,+91-231-2692333 (O); Tel:+91-231-2609338*

bPolymer Energy Materials Laboratory, Advanced Chemical Engineering Department, Chonnam National University, Gwangju, South Korea
c Thin film Materials Loboratory,Department of Physics, Shivaji University,Kolhapur, India.

1   P. V. Kamat, *J. Phys. Chem. C*, 2008, **112**, 18737.
2   M. Husain, B. P. Singh, S. Kumar, T. P. Sharma and P. J. Sebastian, *Sol. Energy Mater. Sol. Cells*, 2003, **76,** 399.
3   R. Xie, J. Su, Y. Liu and L. Guo, *Int. J. Hydrogen Energy*, 2014, **39,** 3517.
4   K.R. Murali and M. Balasubramanian, Curr.*Appl. Phys*., 2010, **10**, 734.
5   Y. Zou, D. Li and D. Yang, *Mater. Chem. Phys.,* 2012, **132**, 865.
6   A. Emrani, P. Vasekar and C. R. Westgate, *Sol. Energy,* 2013, **98,** 335.
7   S. Rubio, J. L. Plaza and E. Diéguez, *J. Cryst. Growth,* 2014, **401**, 550.
8   R. E. Ornelas, D. Avellaneda, S. Shajia, G. A. Castillo, T. K. Das Roy and B. Krishnana, *Appl. Surf. Sci*., 2012, **258**, 5753.
9   K. V. Khot, S. S. Mali, R. R. Kharade, R. M. Mane, P. S. Patil ,C. K. Hong, J. H. Kim, J. Heo and P. N. Bhosale, *J. Mater. Sci: Mater. Electron.,* 2014, **25**, 5606.
10 S. D. Kharade, N. B. Pawar,V. B. Ghanwat, S. S. Mali, W. R. Bae, P. S. Patil, C. K. Hong, J. H. Kim and P. N. Bhosale, *New J. Chem*., 2013, **37**, 2821.
11 S. V. Patil, R. M. Mane, N. B. Pawar, S. D. Kharade, S. S. Mali, P. S. Patil, G. L. Agawane, J. H. Kim and P. N. Bhosale, *J. Mater. Sci. Mater. Electron*., 2013, **24**, 4669.
12 B. D. Ajalkar, R. K. Mane, B. D. Sarwade and P. N. Bhosale, *Sol. Energy Mater. Sol. Cells,* 2004, **81**, 101.
13 A. R. Patil, V. N. Patil, P. N. Bhosale and L. P. Deshmukh, *Mater. Chem. Phys*., 2000, **65**, 266.
14 M. M. Salunkhe, R. R. Kharade, S. D. Kharade, S. S. Mali, P. S. Patil and P. N. Bhosale, *Mater. Res. Bull*., 2012, **47**, 3860.
15 R. M. Mane, S. R. Mane, R. R. Kharade and P. N. Bhosale, *J. Alloys Compd.,* 2011, **491**, 321.
16 V. B. Ghanwat, S. S. Mali, S.D. Kharade, N. B. Pawar, S. V. Patil, R. M. Mane, P. S. Patil, C.K. Hong and P. N. Bhosale, *RSC Adv*., 2014, **4**, 51632.
17 C. P. Liu and C. L. Chuang, *Sol. Energy*, 2012, **86,** 2795.
18 C. A. Arredondo and G. Gordillo, *Phys. B.,* 2010, **405**, 3694.
19 N. G. Dhere , V. S. Gade, A. A. Kadam, A. H. Jahagirdar and S. S. Kulkarni, *Mater. Sci. Eng. B*., 2005, **116,** 303.
20 B. Pejova, *J. Solid State Chem*., 2014, **213**, 22.
21 A. H. Ammar, *Vacuum,* 2001, **60,** 355.
22 M. P. Deshpande, N. Gargn, S. V. Bhatt, P. Sakariya and S. H. Chaki, *Mat. Sci. Semicon. Proc*., 2013, **16,** 915.
23 J. Sharma and S. K. Tripathi, *Phys. B*, 2011, **406,** 1757.
24 M. Dhanam , R. R. Prabhu and P. K. Manoj, *Mater. Chem. Phys*., 2008, **107,** 289.
25 M. Chaudhri, A. Vohr and S. K. Chakarvarti, *Phys. E*, 2008, **40**, 849.
26 H. Wen, C. Yang , W. Chou, *Appl. Surf. Sci*., 2010, **256**, 2128.
27 L. A. Waha, H. A. Zayed, A. A. Abd and El-Galil, *Thin Solid Films* 2012, **520**, 5195.
28 A. H. Ammar, *Phys. B*., 2001, **296**, 312.
29 S. D. Chavhan, R. S. Mane, W. Lee, S. Senthilarasu, S. Han, J. Lee, and S. Lee, *Electrochim. Acta*., 2009, **54,** 3169.
30 Y. G. Gudage and R. Sharma, *Curr. Appl. Phys*., 2010, **10**, 1062.
31 R. B. Kale, C. D. Lokhande, R. S. Mane and S. H. Han, *Appl. Surf. Sci.,* 2007, **253,** 3109.
32 D. S. Sutrave, G. S. Shahane, V. B. Patil and L. P. Deshmukh, *Mater. Chem. Phys.,* 2000, **65,** 298.
33 V. Kishore, V. K. Saraswat, N. S. Saxsena and T. P. Sharma, *Bull. Mater. Sci.,* 2005, **28,** 431.
34 J. Camacho, I. Loa, A. Cantarero, I. H. Calderon and K. Syassen*, Microelectron. J*., 2002, **33,** 349.
35 S. D. Chavhan, R. S. Mane, T. Ganesh, W. Lee, S. H. Han, S. Senthilarasu and S. H. Lee, *J. Alloys Compd*., 2009, **474,** 210.

36 C. X. Shan, X. W. Fan, J. Y. Zhang, Z. Z. Zhang, X. H. Wang, Y. M. Lu, Y. C. Liu, D. Z. Shen and S. Z. Lu, *J. Cryst. Growth, 2004,* **265**, 541.
37 S. D. Chavhan, S. Senthilarasu, J. Lee and S. Lee, *J. Phys. D: Appl. Phys*., 2008, **41,** 165502.
38 B. S. Tosun, C. Pettit, S. A. Campbell and E. S. Aydil, *Appl. Mater. Interfaces*., 2012, **4,** 3676.
39 S. M. Pawar, B. S. Pawar, J. H. Kim , O. S. Joo and C. D. Lokhande, Curr. *Appl. Phys*., 2011, **11,** 117.
40 J. Li and H. C. Zeng, *J. Am. Chem. Soc*., 2007, **129**, 15839.
41 A. U. Ubale, *Mater. Chem. & Phys*., 2010, **121,** 555.
42 D. Litvinov, M. Schowalter, A. Rosenauer, B. Daniel, J. Fallert, W. Löffler, H. Kalt and M. Hetterich, *Phys. Stat. Sol A*., 2008, **205**, 2892.
43 R. Zhai, S. Wang, H. Y. Xu, H. Wang and H. Yan, *Mater. Lett*., 2005, **59**, 1497.
44 X. Wu, Y. Yu, Y. Liu, Y. Xu, C. Liu and B. Zhang, *Angew. Chem. Int. Ed*., 2012, **51**, 3211.
45 B. Schwenzer, J. R. Neilson, S. M. Jeffriesc and D. E. Morse, *Dalton Trans*., 2011, **40**, 1295.
46 Y. Akaltun, M. Ali Yıldırım, A. Atesn and M. Yıldırım, *Mate. Res. Bull*., 2012, **47**, 3390.
47 G. J. Camargo-Gambo, J. S. L. Pacheco, J. M. de Leon, S. D. Conradson and I. Herna´ndez-Caldero, *Thin Solid Films*, 2005, **490**, 165.
48 M. Ashokkumar and S. Muthukuma, *J. Lumin*., 2014, **145,** 167.
49 Z. Deng, H. Yan and Y. Liu, *J. Am. Chem. Soc*., 2009, **131**, 17744.
50 Y. C. Pu and Y. J. Hsu., *Nanoscale*, 2014, **6**, 3881.
51 F. Mezrag, W. K. Mohamed and N. Bouariss, *Phys. B*, 2010 ,**405**, 2272.
52 J. Cao, B. Xue, H. Li, D. Deng and Y. Gu, *J. Colloid Interface Sci*., 2010, **348,** 369.
53 Y. Sheng, J. Weia, B. Liu and L. Peng, *Mate. Res. Bull*., 2014, **57,** 67.
54 Y. Myung, J. H. Kang, J. W. Choi, M. D. Jang and J. Park, *J. Mater. Chem.,* 2012, **22**, 2157.
55 R. Zhang and P. Yang., *J. Phys. Chem. Solids*., 2013, **74**.
56 X. H. Zhong, Y. Y. Feng, W. Knol and M. Y. Han, *J. Am. Chem. Soc*., 2003, **125**, 13559.
57 Z. T. Deng, F. L. Lie, S. Y. Shen, I. Ghosh, M. Mansuripur and A. J. Muscat, *Langmuir*., 2009, **25**, 434.
58 Y. Y. Lee, J. K. Shon, S. Bae, X. Jin,Y. J. Choi, S. S. Kwon, T. H. Han and J. M. Kim, *New J. Chem*., 2014, **38**, 3729.
59 L. Yang, R. Zhou, J. Lan, Q. Zhang, G. Cao and J. Zhu, *J. Mater. Chem. A.,* 2014, **2**, 3669.
60 L. Vegard and H. Schjelderup, *Phys. Z*, 1917, **18**, 93.
61 X. Zhong, Z. Zhang, S. Liu, M. Han and W. Knoll, *J. Phys. Chem. B*., 2004, **108**, 15552.
62 P. B. Patil, S. S. Mali, V. V. Kondalkar, N. B. Pawar, K.V. Khot, C. K. Hong, P. S. Patil and P. N. Bhosale, *RSC Adv*., 2014, **4**, 47278.
63 S. A. Pawar, R. S. Devan, D. S. Patil, A. V. Moholkar, M. Gil Gang, Y.Mab, J. Kim and P. S. Patil, *Electrochim. Acta*., 2013, **98,** 244.
64 T. Liu,Y. Hua and W. Chang, *Mat Sci Eng B*, 2014, **180**, 33.
65 J. Pouzet and J. C. Bernede, *Revue Phys. Appl.,* 25 (1990) 807.
66 J. Newman, Electrochemical System 3rd edition *ISBN: 978-0-471- 477563*, May 2004.
67 S. A. Vanalakar , M. P. Suryawanshi , S. S. Mali , A. V. Moholkar , J. Y. Kim, P. S. Patil and J. H. Kim, *Curr. Appl. Phys*., 2014, **14**, 1669.
68 S. D. Kharade, N. B. Pawar , S. S. Mali ,C. K. Hong, P. S. Patil, M. G. Gang, J. Kim and P. N. Bhosale, *J. Mater Sci.,* 2013, **48**, 7300.

A facile and low cost strategy to synthesize $Cd_{1-x}Zn_xSe$ thin films for photoelectrochemical performance: Effect of zinc content

Chaitali S. Bagade,[a] Sawanta S. Mali,[b] Vishvanath B. Ghanwat,[a] Kishorkumar V. Khot,[a] Pallavi B. Patil,[a] Suvarta D. Kharade,[a] Rahul M. Mane,[a] Neha D. Desai,[a] Chang K. Hong,[b] Pramod S. Patil[c] and Popatrao N. Bhosale*[a]

[a] *Materials* Research *Laboratory, Department of Chemistry, Shivaji University,Kolhapur, India. E-mail:*

p_n_bhosale@rediffmail.com;

Fax:+91-231-2691533,+91-231-2692333 (O); Tel:+91-231-2609338

[b] *Polymer Energy Materials Laboratory, Advanced Chemical Engineering Department, Chonnam National University, Gwangju, South Korea*

[c] *Thin film Materials Loboratory,Department of Physics, Shivaji University,Kolhapur, India*

Graphical abstract